Through-thickness resolution, stress oscillations and residual stress in cold rolling

Francis Flanagan[a], Alison N. O'Connor[b,c], Mozhdeh Erfanian[d,e], Omer Music[f,g], Edward J. Brambley[d,e,*], Doireann O'Kiely[a,*]

[a] *Mathematics Applications Consortium for Science and Industry (MACSI), Department of Mathematics & Statistics, University of Limerick, Limerick, V94 T9PX, Ireland*
[b] *Computer Science and Information Systems (CSIS), University of Limerick, Limerick, V94 T9PX, Ireland*
[c] *Lero, The Science Foundation Ireland Centre for Software Research, University of Limerick, Limerick, V94 T9PX, Ireland*
[d] *Mathematics Institute, University of Warwick, Coventry, CV4 7AL, UK*
[e] *WMG, University of Warwick, Coventry, CV4 7AL, UK*
[f] *Department of Engineering, University of Cambridge, Cambridge, CB2 1PZ, UK*
[g] *Mechanical Engineering Department, TED University, Ankara, Turkey*

Published in European Journal of Mechanics — A/Solids, volume ???, 105761 (2025),
doi:10.1016/j.euromechsol.2025.105761

Abstract

Metal rolling is a widespread and well-studied process, and many finite-element (FE) rolling simulations can be found in the scientific literature. However, these FE simulations are typically limited in their resolution of through-thickness variations. In this paper, we carefully assess the accuracy of a number of FE approaches, and find that at least 60 elements through-thickness are needed to properly resolve through-thickness variation; this is significantly more than is used elsewhere in the metal rolling literature. In doing so, we reveal an oscillatory stress pattern, which is not usually observed in simulations but which we can validate by comparison with recent analytical work, and which is completely deterministic, not arising from numerical noise or error. We discuss the physical basis of these oscillations and their implications for outcomes such as curvature in asymmetric rolled sheets. Accurate through-thickness variation of stress and strain will also have implications for modelling of microstructure evolution and damage.

Keywords: finite element, plasticity, elasticity, cold rolling, residual stress.

1. Introduction

In cold rolling, a sheet of metal, whose temperature is below the material recrystallisation temperature, is gradually fed between two rotating rollers. The rollers are held at a fixed separation that is less than the initial thickness of the sheet and act to permanently deform the sheet so that its thickness is reduced as illustrated in Figure 1. Mathematical models of the cold-rolling process have been used for many years to make predictions, optimise system design and tighten process specification (Orowan, 1943; Horton and Allwood, 2017; Wehr et al., 2020). Waste reduction is also an important motivator in this context as the production of steel and aluminium grows year-on-year and is a major contributor to global energy consumption and CO_2 emissions (Milford et al., 2011; Allwood et al., 2016; World Steel Association, 2024).

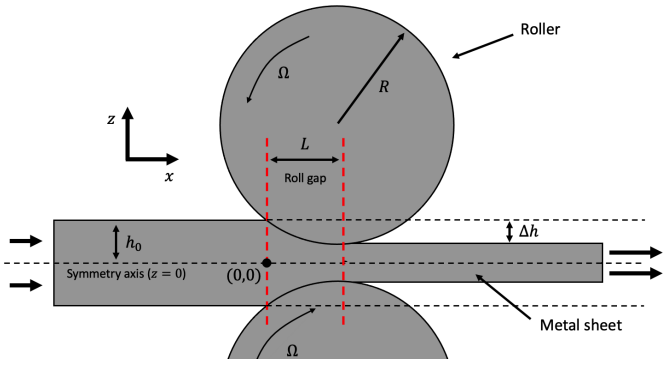

Figure 1: Schematic of the metal rolling process. The sheet moves from left to right and its thickness is reduced by the roller. Symmetry about the centre of the sheet ($z = 0$) is assumed, so only the top roller and top half of the sheet are modelled in this work.

In this paper we study cold rolling using finite element (FE) analysis, but go beyond the previous literature by focusing in detail on through-thickness variations. We show that rolled sheets contain a rich and detailed stress pattern with repeating oscillations that have not been properly resolved previously. These oscillations do not

*Corresponding Authors
Email addresses: Francis.Flanagan@ul.ie (Francis Flanagan), Alison.OConnor@ul.ie (Alison N. O'Connor), Mozhdeh.Erfanian@warwick.ac.uk (Mozhdeh Erfanian), om236@cantab.ac.uk (Omer Music), E.J.Brambley@warwick.ac.uk (Edward J. Brambley), Doireann.OKiely@ul.ie (Doireann O'Kiely)

(a)

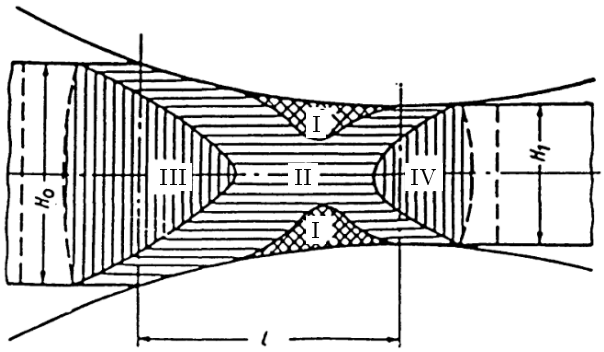

(b)

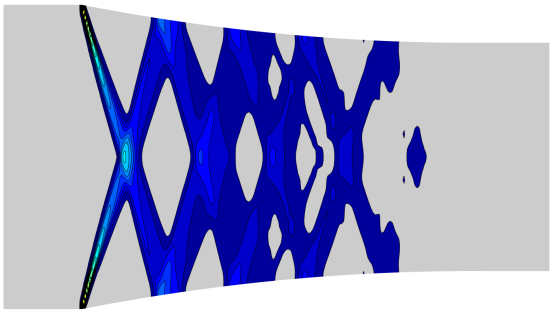

Figure 2: Deformation zones in a metal sheet during rolling: (a) deformation zones reported by Tarnovskii et al. (1965). Region I has "restricted deformation", II has thinning, and III and IV have thickening. (b) PEEQ rate predicted here. Grey zones are not flowing, even if they are at yield, while darker zones are shearing. The thickness-to-length ratio of the roll gap is $O(1)$ in (a) and 1/8 in (b).

arise from noise, vibrations or uncertainty, but rather are completely deterministic. Furthermore, these oscillations have implications for the existence of deforming and non-deforming zones inside the roll gap (see Figure 2a) and for the downstream properties of rolled metal sheets. The research aims of this paper are as follows:

1. Assess the suitability of typical FE models for resolving through-thickness variations in metal sheet rolling.
2. Systematically develop an FE modelling approach which fully resolves internal stress patterns, with validation.
3. Use the FE model to predict and investigate stress oscillation patterns inside the roll gap during metal sheet rolling, as well as through-thickness variation of residual stress in rolled metal sheets.

In Section 2, we investigate predictions of through-thickness stress and strain variations in existing FE and analytical models. In Section 3 we outline the specifics of the metal rolling process considered here together with the implicit and explicit analyses considered in ABAQUS. We conduct a mesh study and compare implicit and explicit models in terms of their ability to accurately predict through-thickness stress variations. We also show that roll force and torque are poor determinants of the optimal mesh size and of the steady state condition. In Section 4 we present predictions of stress and deformation generated by our FE simulations, with an emphasis on quantifying oscillatory mechanics inside the roll gap. In Section 5 we provide a physical interpretation of our observations, as well as further validation, by comparison with a new analytical model from Erfanian et al. (2024). In Section 6 we draw conclusions and briefly discuss the future plans for our FE simulations.

2. Literature review

Significant effort has been devoted to modelling a rich variety of complexity in rolling processes in the engineering lieterature (Montmitonnet et al., 2016; Hu et al., 2021). Here we provide an overview of some existing analytical and FE rolling models that consider through-thickness variations in their analyses, and demonstrate their strengths and limitations. Early mathematical descriptions of cold rolling used a "slab" approach pioneered by Orowan (1943). Slab models treat the sheet as a series of vertical slabs, assuming the slabs remain vertical throughout the rolling process and that stresses are uniform across the sheet thickness. While this simple mathematical description can yield reasonably accurate predictions of the roll force and torque required for a given thickness reduction, they automatically disregard any through-thickness effects (Minton et al., 2016). Experimental observations of deformation led to pictures like the one shown in Figure 2(a), as outlined in §2.1, with zones of thinning, thickening and restricted deformation, clearly demonstrating through-thickness variations in the flow profile of a metal sheet undergoing rolling. Through-thickness variations in both stress and strain can in principle be described with more advanced modelling techniques such as FE analysis (Thompson, 1982; Mori et al., 1982; Yarita et al., 1985; Lau et al., 1989; Yoshii et al., 1991; Richelsen, 1997; Ghosh et al., 2004; Gudur and Dixit, 2008; Lenard, 2013; Cawthorn et al., 2014; Minton, 2017), but only at sufficiently high resolution, as outlined in §2.2, while advanced mathematical analysis can improve on slab theory in certain regimes, as outlined in §2.3

2.1. Experimental literature

Over the last century, experimental approaches to studying rolling included cutting grooves on the sides of steel, aluminium and copper bars, rolling and then cutting open multicolored plasticine bars, and embedding pins or other inserts in metal sheets in order to observe deformations or, where feasible, strains (Orowan, 1943; Tarnovskii et al., 1965; Hartley et al., 1989; Boldetti

et al., 2005). Most recently, Digital Image Correlation (DIC) has emerged as a technique for more accurately tracking deformation at a sheet's outer edge (Jacobs et al., 2022; Hoefnagels et al., 2022). The different techniques expose through-thickness variations either in the interior or at the edge of a sheet during rolling. For example, groove-cutting by Tarnovskii and co-authors yielded the hypothesized deformation zones in Figure 2(a) (Tarnovskii et al., 1965), while time-integrated DIC was used by Hoefnagels and co-authors to estimate velocities and strains during rolling (Hoefnagels et al., 2022). In both cases, some through-thickness variations can be observed in the experimental observations, although the resolution of these observations is limited by the number of grooves or, in the case of DIC, the order of polynomial used in image post-processing.

2.2. FE literature

Table 1 summarizes the level of through-thickness variation presented in existing FE models in the literature, noting the different numerical approaches used (e.g., 2D or 3D simulation, number of elements through-thickness ($2N_e$), element type etc.). While several authors report shear stress along the roller-sheet interface (Lindgren and Edberg, 1990; Richelsen, 1996; Cawthorn et al., 2016), Table 1 shows that few (Yarita et al., 1985; Cawthorn et al., 2014; Minton, 2017) provide the through-thickness shear stress variation. Given the potential implications of oscillating shear stress on downstream quantities such as residual stress (Erfanian et al., 2023; Flanagan et al., 2023), we argue that a "good" FE model should be capable of accurately predicting the oscillatory shear stress (and other quantities) through the thickness of the sheet.

Yarita et al. (1985) plotted the shear stress versus position in the rolling direction at four different heights from the sheet centre to the surface, since stresses were computed with $N_e = 4$ reduced-integration quadrilateral elements through the half-thickness of the sheet. Although some through-thickness variation is observed, we will see in §3.6 that this mesh is far too coarse to resolve these variations accurately. Oscillations are visible in the shear stress curves but were not mentioned in the text. Similarly, Cawthorn et al. (2014) use $N_e = 5$ reduced-integration elements in their ABAQUS/Explicit FE model, which is too coarse for accurate resolution.

Minton (2017) considered a range of roll-gap shapes, and noted the emergence of an oscillatory pattern in shear, where the number of lobes in the oscillatory pattern is proportional to the aspect ratio of roll-gap length to thickness. In the limit of a long roll gap, many oscillatory lobes blur together so that none are visible, while a single sign change in shear occurs when the roll gap length and width are the same, consistent with most analytical models. Indeed, the author hypothesizes that the simplified phenomenology in these limiting cases may explain why this oscillatory pattern has been largely missed in the literature — for example, the aspect ratio in the experiments leading to Figure 2(a) was close to 1, appropriately yielding a single "oscillation". We note that the mesh used by Minton (2017) was still relatively coarse, with $N_e = 9$–15, and that the means of determining a steady state is by analysing roll force and torque, which we will see below is a poor steady-state predictor (c.f. §3.7).

Elsewhere in the literature, Olaogun et al. (2019) focus on the role of temperature and find an oscillatory pattern in their heat flux contour plots. During plastic flow, mechanical energy is dissipated as heat, and plastic flow takes place in metals predominantly by shearing (Howell et al., 2009), so one might reasonably expect a relationship between the heat flux oscillations observed by Olaogun et al. (2019) and any shear stress oscillations that exist during rolling. Finally, many other authors have illustrated through-thickness variation but only via quantities that are not significantly oscillatory, such as longitudinal stress, effective stress or equivalent strain (Thompson, 1982; Mori et al., 1982; Lau et al., 1989; Yoshii et al., 1991; Richelsen, 1997; Ghosh et al., 2004; Gudur and Dixit, 2008; Lenard, 2013). Others report through-thickness variations via mesh distortion (Mori et al., 1982; Lau et al., 1989; Liu et al., 1987). Tadić et al. (2023) study the longitudinal residual stress induced by cold rolling through-thickness inhomogeneities via FE analysis, and state that it is "imperative" to determine the through-thickness stress distributions during cold rolling to accurately predict and control the impact of longitudinal residual stress on the appearance and properties of cold-rolled strips. However, Tadić et al. (2023) select their mesh density ($N_e = 8$) by satisfying convergence conditions concerning the mean value of the contact stress. We will see in subsection 3.6 that accurate measurements of such surface quantities does not imply accurate through-thickness predictions, and that higher resolution is required when through-thickness predictions are desired. Li and Kobayashi (1982) present contour plots of shear strain rate at a low resolution inhibiting any oscillatory pattern observation. Liu et al. (1988) presented cross-sectional profiles of strain components from three-dimensional simulations which contain hints of oscillations but these patterns are not commented on. The results of Misovic et al. (2016) for displacement and velocity also hint at a possibility of oscillations, but are only presented at the sheet centre and surface.

It is clear that a reliable FE model, one capable of accurately predicting through-thickness stress and strain variations, is absent from existing literature. We aim to provide such a model, which can be used to guide and compare with faster analytical models.

Table 1: Summary of FE models in the literature that consider through-thickness variations. Note that $2N_e$ represents the number of elements through the full thickness of the sheet, PEEQ is plastic equivalent strain and the material models are elastic-plastic (EP), rigid-plastic (RP), elasto viscoplastic (EVP) and elastoplastic (EoP). The * indicates that oscillations are visible in certain FE results, but are not directly discussed in the paper.

Reference	**2D or 3D**	$2N_e$	**Element type**	**Material model**	**Through-thickness variations**	**Symmetric system**	**Oscillatory pattern**
Current work	2D	10–80	Plane-strain 4-node, reduced-integration	EP	Shear, von Mises, PEEQ, PEEQ rate	✓	✓
Li and Kobayashi (1982)	2D	10		RP	Mesh distortion, relative velocities, normal/shear strain rates, PEEQ	✓	
Thompson (1982)	2D	12	Six-node triangular	EVP	Effective stress	✓	
Mori et al. (1982)	2D	10	Isoparametric quad full integration	RP	Mesh distortion, PEEQ rate, normal stress	✓	
Liu et al. (1985)	3D	8–10	8-node brick	EP	Velocity flow patterns	✓	
Yarita et al. (1985)	2D	8	Quad, reduced-integration	EP	Stress components	✓	✓*
Liu et al. (1987)	3D	6		EP	Mesh distortion	✓	
Mori and Osakada (1987)	2D	14	Quad	RP	PEEQ rate, pressure	✓	
Liu et al. (1988)	3D	3	8-node brick	EP	Incremental strain components	✓	✓*
Lau et al. (1989)	2D	20	Quad	EP	Mesh distortion, PEEQ	✓	
Yoshii et al. (1991)	2D	8		RP	PEEQ, PEEQ rate	Asymmetric	
Malinowski and Lenard (1992)	2D	18	4-node	EoP	Stress (centre & surface only)	✓	
Richelsen (1997)	2D	18	Quad	EVP	Mesh distortion, PEEQ, horizontal stress	Asymmetric	
Ghosh et al. (2004)	3D	10	8-node brick, reduced-integration	EP	Effective stress, PEEQ	✓	
Gudur and Dixit (2008)	2D	8	Rectangular	RP	PEEQ	✓	

Shahani et al. (2009)	2D	16–18	Plane-strain 4-node	VP	Temperature, strain, strain rate, effective stress	✓	
Lenard (2013)	2D		Isoparametric quad elements	EP	PEEQ	✓	
Cawthorn et al. (2014)	3D	10	8-node brick reduced-integration	EP	Vertical, shear stress components	✓	
Zhou et al. (2016)	3D	12	8-node brick reduced-integration temperature-coupled	EP	Normal stress, pressure, displacements (edge only)	✓	
Misovic et al. (2016)	2D	16	Square isoparametric	RP	PEEQ, displacements, velocities	✓	✓*
Koohbor and Moaven (2017)	2D	36	3-noded triangular	RP	PEEQ, temperature	✓	
Minton (2017)	Both	2D: 18-30, 3D: 11	2D: Plane-strain 4-node reduced-integration, 3D: 8-node reduced-integration	EP	Stress, velocity components	Symmetric and asymmetric	✓
Olaogun et al. (2019)	2D	20	4-node isoparametric	EP	Temperature, heat flux	✓	✓
Tadić et al. (2023)	2D	16	4-node square elements	EP	Longitudinal, shear and effective strain, longitudinal and von Mises stress	✓	
Flanagan et al. (2023)	2D	12–100	Plane-strain 4-node reduced-integration	EP	Vertical velocity, von Mises	✓	✓

2.3. Mathematics literature

Asymptotic analysis is useful for modelling physical processes where the smallness (or largeness) of a fundamental process parameter can be exploited (Murray, 2012). This type of analysis is particularly useful for cold rolling, where the roll-gap aspect ratio is typically large (Cawthorn et al., 2016), i.e., $1/\varepsilon = L/h_0 \gg 1$, where h_0 is the initial half-thickness of the sheet and $L = \sqrt{2R\Delta h}$ is the approximate horizontal length of the roll gap (see Figure 1). Domanti and McElwain (1995) assume a small reduction in the sheet's thickness (i.e., $r = \Delta h/h_0 \ll 1$) along with the large-aspect-ratio assumption. These assumptions enable an asymptotic analysis to be carried out to obtain accurate solutions in the limits as $\varepsilon \to 0$ and $r \to 0$. Erfanian et al. (2024) relax the assumption that the reduction of the sheet thickness is small and also resolve behaviour over two distinct length scales associated with h_0 and L. By contrast, Domanti and McElwain (1995) and other authors (see, for example, Cawthorn et al., 2016) consider variations on a length scale of L only. The multiple-scales analysis of Erfanian et al. (2024) recovers slab theory at leading order, and at higher orders predicts through-thickness oscillations in stress and velocity in the roll gap. These through-thickness variations have also been captured by the current authors in a preliminary conference proceedings (Flanagan et al., 2023). Note that the Erfanian et al. (2024) model is limited to rigid-perfectly-plastic materials, while FE models can integrate elastic-plastic material behaviour to capture elasticity and strain hardening.

3. Simulation details

In this section we outline the FE models used in this work. A more pedagogical presentation of how they work can be found in the Supplementary Material (Section 1, drawing on references (Tarnovskii et al., 1965; Minton, 2017; Lindgren and Edberg, 1990; Cawthorn et al., 2016; Hadadian and Sedaghati, 2019; Dassault Systémes, 2021; Jiang and Tieu, 2002; Natário et al., 2014; Gavalas et al., 2018; Padhye, 2023; Min et al., 2006; Ktari et al., 2012; Edberg and Lindgren, 1993; Díaz et al., 2021; Jung and Yang, 1998).) We include key information about the geometry, material, dynamics, mesh, contact and computer precision settings.

3.1. Model geometry

Since the metal sheet's width–thickness ratio is, in general, large in cold rolling (e.g. Hacquin et al. (1996); Yao et al. (2019, 2020) all employ a width–thickness ratio that is at least 100), we consider an idealised two-dimensional geometry by assuming plane-strain conditions apply (in line with Lenard, 2013; Richelsen, 1996; Jacobs et al., 2023). We use the model geometry illustrated in Figure 1, considering the top half of the sheet only and assuming symmetry about $z = 0$. We consider a rigid roller of radius $R = 257.45\,\text{mm}$, rolling a sheet of initial half-thickness $h_0 = 2\,\text{mm}$, and impose an approximate half-thickness reduction of $\Delta h = 0.5\,\text{mm}$. This corresponds to $\varepsilon = h_0/L = 0.125$, where $L = 16.05\,\text{mm}$ is the approximate horizontal length of the roll gap.

3.2. Material properties

We consider a sheet of elastic-plastic mild steel (grade DC04) (Spittel and Spittel, 2009); this deforms elastically up to an initial yield stress of $Y = 477.2\,\text{MPa}$, and the yield stress increases to 650.25 MPa at a true plastic strain of 1.1 as a result of strain hardening. The Young's modulus and Poisson's ratio are taken to be $E = 206.3\,\text{GPa}$ and $\nu = 0.3$ respectively. For all explicit analyses, the density of the material is defined as $\rho = 7831.3\,\text{kg}\,\text{m}^{-3}$.

3.3. ABAQUS solver and elements

FE simulations reported in this work were conducted using ABAQUS 2021 (Dassault Systémes, 2021). ABAQUS software offers both implicit and explicit solvers. For cold rolling it is not immediately clear which solution type is better, so we investigate both possibilities in depth in the Supplementary Material (Section 2, drawing on references (Lindgren and Edberg, 1990; Flanagan et al., 2023; Olaogun et al., 2019; Malinowski and Lenard, 1992; Shahani et al., 2009; Hadadian and Sedaghati, 2019; Dassault Systémes, 2021; Shangwu et al., 1999; Safaei and De Waele, 2011; Qiao et al., 2016; Sun, 2006; Souto et al., 2022; Zhang et al., 2022; Yang et al., 2019; Matsubara et al., 2024; Gao et al., 2024; Qian et al., 2010)). In our explicit analysis, numerical noise appears with increasing mesh resolution; we attribute this to the lack of convergence checks performed by ABAQUS/Explicit at each time step. These artefacts can be removed by implementing additional stiffness-proportional damping (Flanagan et al., 2023), but in light of this divergence and the lack of equilibrium checks, we use ABAQUS/Standard for our analysis. In a detailed investigation presented in the Supplementary Material, we find that a standard implicit analysis (CPE4 elements) suffers from shear locking when the resolution is increased to the level we require. This can be overcome using either "incompatible" elements (CPE4I) or plane-strain reduced-integration elements (CPE4R). The incompatible elements increase computational time to an extent that severely limits the mesh resolution we can feasibly achieve, so we use reduced-integration (CPE4R) elements for this analysis.

3.4. General FE model conditions

We first initialize sheet–roller contact in a *bite* step, and subsequently rotate the roller to deform and translate the sheet in a *rolling step*. To ensure contact convergence between the sheet and the roller, the bite step occurs over a time increment of 1 s. The rolling step occurs over a time increment of 0.1 s. This is enough time for approximately

Feature	Setting
Step type	Static, general
Amplitude curve	Instantaneous
Contact tracking	State-based
Contact discretisation	Surface-to-surface

Table 2: FE model settings.

8 roll-gap lengths to be rolled when $R = 257.45\,\text{mm}$. No tension is applied at the sheet ends.

The sheet's horizontal centre line (i.e., the symmetry axis in Figure 1) is constrained vertically to enforce the expected symmetry. This modelling choice reduces the computational intensity of the problem, and in turn facilitates the use of a finer mesh. The centre of the roller is defined as a reference point and boundary conditions, depicting the movement of the roller, are applied to this location. Initially, the roller and the sheet are not in contact, but are set up such that the roller is positioned above the sheet. In the bite step the roller is slowly translated vertically (via a velocity boundary condition) to indent the sheet, but no rotation of the roller occurs in the bite step. In the rolling step, the roller reference point is fixed so its only degree of freedom is rotation in the rolling direction, and the roller is given a tangential velocity of $R\Omega = 1287.25\,\text{mm}\,\text{s}^{-1}$ (corresponding to an angular velocity $\Omega = 5$ rad s^{-1}, applied instantaneously). A bite step is used here, instead of starting the strip in front of the roll gap and feeding it in in some way, as the bite-then-roll simulations showed fewer initial contact issues and converged more quickly to steady state (as also described by Minton, 2017).

Our FE model settings are summarized in Table 2. To ensure computational precision, full nodal output was requested for all simulations in this work. This is equivalent to double precision in explicit simulations. Meshing is applied using a global seed formulation with a structured meshing technique. Varying levels of mesh density were considered and the optimal mesh is discussed in detail in §3.6.

3.5. Contact conditions

We assume the roller is rigid and define it as the main surface for contact between the roller and the sheet. The deformable sheet surface is then defined as the secondary surface. Hard pressure-overclosure contact is the most common contact pressure–overclosure relationship (Dassault Systémes, 2021) and, in principle, has zero contact pressure until contact occurs, whereupon it immediately increases to infinity to prevent penetration. In practice, however, this infinite spike in contact pressure is numerically challenging, and so the zero-penetration condition may or may not be strictly enforced depending on the constraint enforcement method used. Here, we use ABAQUS' default penalty constraint enforcement method, which approximates hard pressure-overclosure behavior, so some degree of penetration will occur.

Elements per half-thickness	CPU time (hours)	von Mises stress	shear stress	PEEQ
5	0.25	20.55%	45.48%	7.24%
10	1.16	12.97%	24.3%	4.33%
15	3.2	9.74%	14.51%	2.93%
20	7.09	5.71%	9.24%	2.02%
30	15.89	3.68%	4.9%	1.09%
40	76.75	-	-	-

Table 3: Compute time and error in simulations with $N_e = 5$–30, benchmarked against a simulation with $N_e = 40$. Errors are given as the maximum deviation relative to the maximum absolute value inside the roll gap.

For cold-rolling processes we expect significant relative motion between the rigid roller and the deformable sheet. To account for relative motion between the roller and sheet surfaces, a finite sliding formulation is adopted. Friction between the roller and the sheet is defined through the isotropic Coulomb friction model, which is regularly used in FE simulations of rolling (e.g., (Mori et al., 1982; Yoshii et al., 1991; Gudur and Dixit, 2008; Minton, 2017; Li and Kobayashi, 1982)). For industrial cold rolling mills the friction coefficient typically lies in the range of $\mu = 0.02 - 0.15$ (Mang, 2014); in this work we use $\mu = 0.1$.

3.6. Mesh sensitivity study

We carry out a mesh convergence study for implicit simulations with CPE4R elements, ranging the mesh density from 5 to 40 elements through the sheet half-thickness. The simulation with 40 elements through-half-thickness has a CPU time on the order of days (see Table 3) so has limited usability practically, but is useful for benchmarking lower-mesh-density simulations.

We run FE numerical simulation with different numbers of elements through the sheet half-thickness ($N = 5$, 10, 15, 20, 30 and 40), and extract the von Mises stress, shear stress and PEEQ (plastic equivalent strain) at three representative distances through the roll gap ($x = 0.025\,L$, $x = 0.6913\,L$ and $x = 1.09\,L$, illustrated in Fig. 3a)[1]. These quantities are plotted as a function of vertical distance from the sheet mid-surface in Fig. 3(b–d). It is immediately apparent that the $N_e = 5$ and in some cases $N_e = 10$ results have substantial qualitative and quantitative differences from the higher-resolution results. For example, the $N_e = 5$ simulations do not capture non-monotonicity in the von Mises stress at $x = 1.09L$ (dashed lines in Fig. 3b), the shear stress at $x = 0.6013L$ has the

[1] These specific positions are chosen because they correspond to the positions of maximum relative error in the three quantities of interest; see Fig. S5 in the Supplementary information for errors as a function of horizontal position.

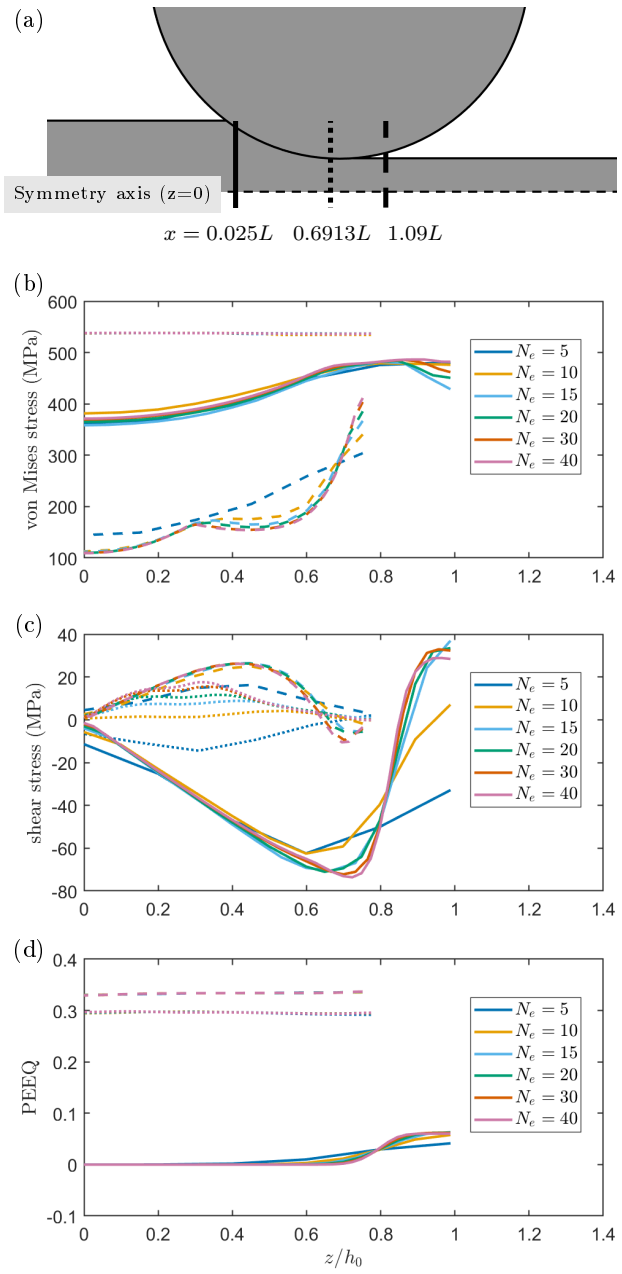

Figure 3: FE simulations are compared by interpolating along vertical lines at $x = 0.025\,L$, $0.6913\,L$ and $1.09\,L$, depicted with solid, dotted and dashed lines respectively in (a). These are the three x-positions with the largest errors (Supplementary Material). Von Mises stress (b), shear stress (c), and PEEQ (plastic equivalent strain, d), are shown as a function of distance from mid-surface, evaluated the positions shown in (a) with the line types shown in (a), for simulations with different numbers of elements through half-thickness ($N_e = 5$, 10, 15, 20, 30, 40), with roller radius $R = 257.45\,\text{mm}$ and roll gap aspect ratio $1/\varepsilon = 8$.

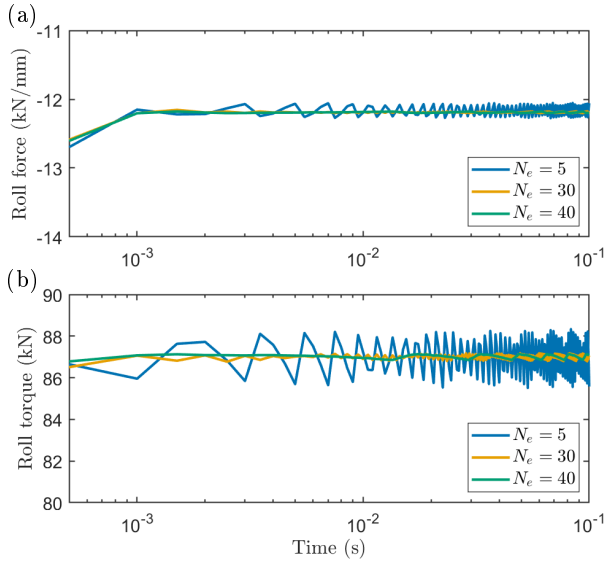

Figure 4: Time-history plots of (a) roll force and (b) torque per unit width during the *rolling* analysis step for implicit simulations with $N_e = 5$, $N_e = 30$ and $N_e = 40$ CPE4R elements. Relatively steady average force and torque values are observed after 0.001 s for each simulation. All simulations have radius $R = 257.45\,\text{mm}$ and $\varepsilon = 0.125$.

incorrect sign (dotted lines in Fig. 3c) and low-and-high PEEQ zones are not properly captured at $x = 0.025L$ (solid lines in Fig. 3d). It is notable, therefore, that Yarita et al. (1985) and Cawthorn et al. (2014) used $N_e = 4$ and $N_e = 5$ reduced-integration elements respectively through the half-thickness of the sheet, which our results suggest is too coarse a mesh to accurately capture the through-thickness stress and strain distributions in the sheet.

We complete our mesh convergence study by calculating the error for $N_\text{e} < 40$ relative to $N_\text{e} = 40$ simulations. Results are interpolated in the z-direction to facilitate comparison between different mesh densities. The error in all three quantities (von Mises stress, shear stress and PEEQ) is below 5% for $N_\text{e} = 30$, and we use this mesh for simulations in the remainder of the study below.

Finally, we note that the roll force and roll torque have the same average value for $N_\text{e} = 5$ as for $N_\text{e} = 30$, 40, albeit with some oscillations in time (see Figure 4. Using these quantities as measure of mesh convergence, as is common in the literature, would have suggested that $N_\text{e} = 5$ is sufficient mesh resolutions. Roll force and roll torque are therefore not suitable measures of convergence when through-thickness variations are of interest.

3.7. Steady-state determination

In Section 2 we noted that steady-state checks in FE simulations are often defined in terms of roll force and/or roll torque in the literature. Figure 4 suggests that for all mesh sizes, these quantities reach a platueau (up to some repeating oscillations in the case $N_\text{e} = 5$) by time

$t \approx 0.001\,\mathrm{s}$. Here we carry out a more indepth study of time convergence, demonstrating that steady roll force and torque does not reliably reflect a steady internal stress state. We extract von Mises stress, shear stress and PEEQ at five timepoints ($t = 0.001\mathrm{s}$, $0.0022\mathrm{s}$, $0.0033\mathrm{s}$, $0.0802\mathrm{s}$, $0.0901\mathrm{s}$, $0.1\mathrm{s}$) at three distances through the roll gap ($x = 0.025\,L$, $x = 0.6913\,L$ and $x = 1.09\,L$, illustrated in Fig. 3a). These quantities are plotted as a function of vertical distance from the sheet mid-surface in Fig. 5. It is immediately apparent that the internal stresses and strains at $x = 1.09L$ are far from steady at $t = 0.0011$; this is notable because the roll force and torque are already steady by this time. More generally, the stresses and strains at all three horizontal positions are indistinguishable to the naked eye for $t \geq 0.0802\,\mathrm{s}$. We extract the data used for the remainder of this paper at $t = 0.0802\,\mathrm{s}$ to both ensure steady results and to facilitate velocity calculations in postprocessing.

4. Numerical results

In this section, we present some notable outputs from our FE simulations, highlighting the emergence of a deterministic oscillatory pattern in the shear, PEEQ rate and velocity profiles of metal sheets during cold rolling. The PEEQ rate and velocities are computed during post-processing, via a method outlined in the Supplementary Material (Section 4). We also compute the residual stress in the sheet after rolling and discuss its connection to the oscillatory pattern in stress and strain quantities in the roll gap. This connection is likely to have a strong relationship with curvature in asymmetric rolling, a phenomenon that is often incorrectly predicted (Minton and Brambley, 2017).

4.1. Oscillations

4.1.1. Shear lobes

The left column of Figure 6 shows our FE prediction of shear stress in sheets undergoing rolling in three different roll gaps corresponding to aspect ratios $1/\varepsilon = 1/0.175$, $1/0.125$ and $1/0.075$. In each of the three cases, we observe a clear oscillatory pattern, with the shear stress varying from -150MPa to $+150$MPa, and with lobes of positive and negative shear stress appearing with regular spacing on both sides of the sheet mid-surface. The number of lobes increases as $1/\epsilon$ increases, which is consistent with preliminary findings from Minton (2017). These lobes are not typically reported in FE modelling of cold rolling (c.f. Table 1) and could be mistaken for numerical error, but they have also been predicted by recent analytical work (c.f. the right column of Figure 6 and Section 5.2).

4.1.2. Deforming and non-deforming zones

Figure 7 shows von Mises stress and PEEQ rate contour plots, along with the sheet's surface and central velocity magnitudes, for the simulation presented in

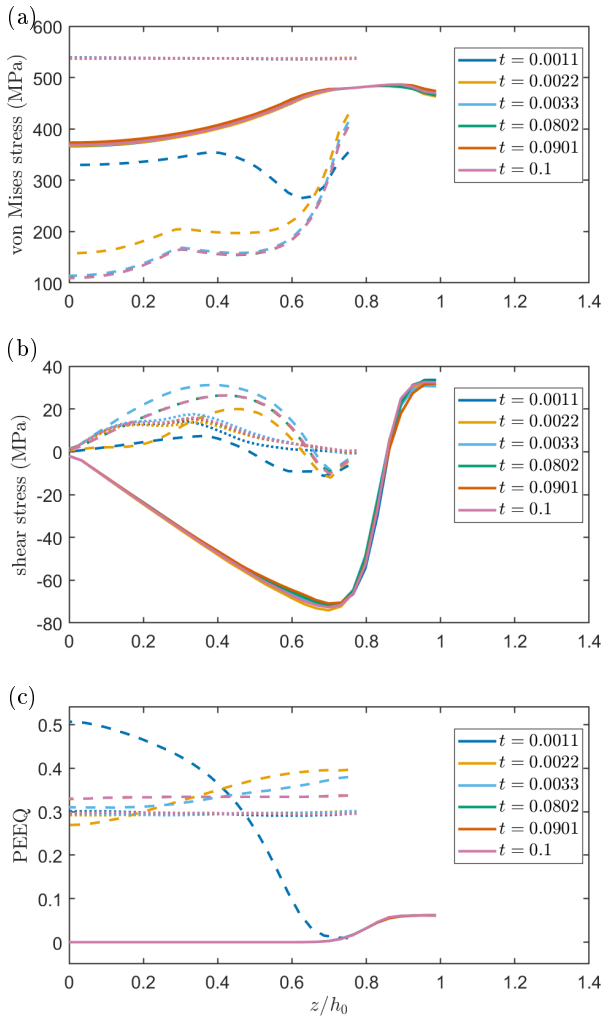

Figure 5: Von Mises stress (a), shear stress (b), and PEEQ (plastic equivalent strain, c), as a function of distance from mid-surface, evaluated at horizontal positions $x/L = 0.025$ (solid lines), 0.6913 (dotted lines) and 1.09 (dashed lines) at different time points $t = 0.0011$, 0.022, 0.0033, 0.0802, 0.0901, 0.1. Simulations are carried out with $N_\mathrm{e} = 30$ CPE4R elements for roller radius $R = 257.45\,\mathrm{mm}$ and roll gap aspect ratio $1/\varepsilon = 8$.

Figure 6(b) ($R = 257.45\,\mathrm{mm}$, $\varepsilon = 0.125$). From Figure 7(a), we see that the von Mises stress does not drop below yield in the interior of the roll gap, as expected. However, the PEEQ rate plot in Figure 7(b) reveals a far richer and more complex layer of dynamics. A clear wave-like structure can be seen, mirroring the oscillatory pattern in shear in Figure 6. The plastic deformation is highly localized in very thin bands, oriented diagonally and oscillating back and forth across the sheet. In the regions between these bands, where the PEEQ rate is zero, the material appears to translate as a solid body, with no plastic flow, even though it is at yield. This is unexpected and may have major implications for hardening and the development of microstructure in the rolled sheet.

We investigate the emergence of rapidly-deforming and non-deforming zones further by plotting the velocity

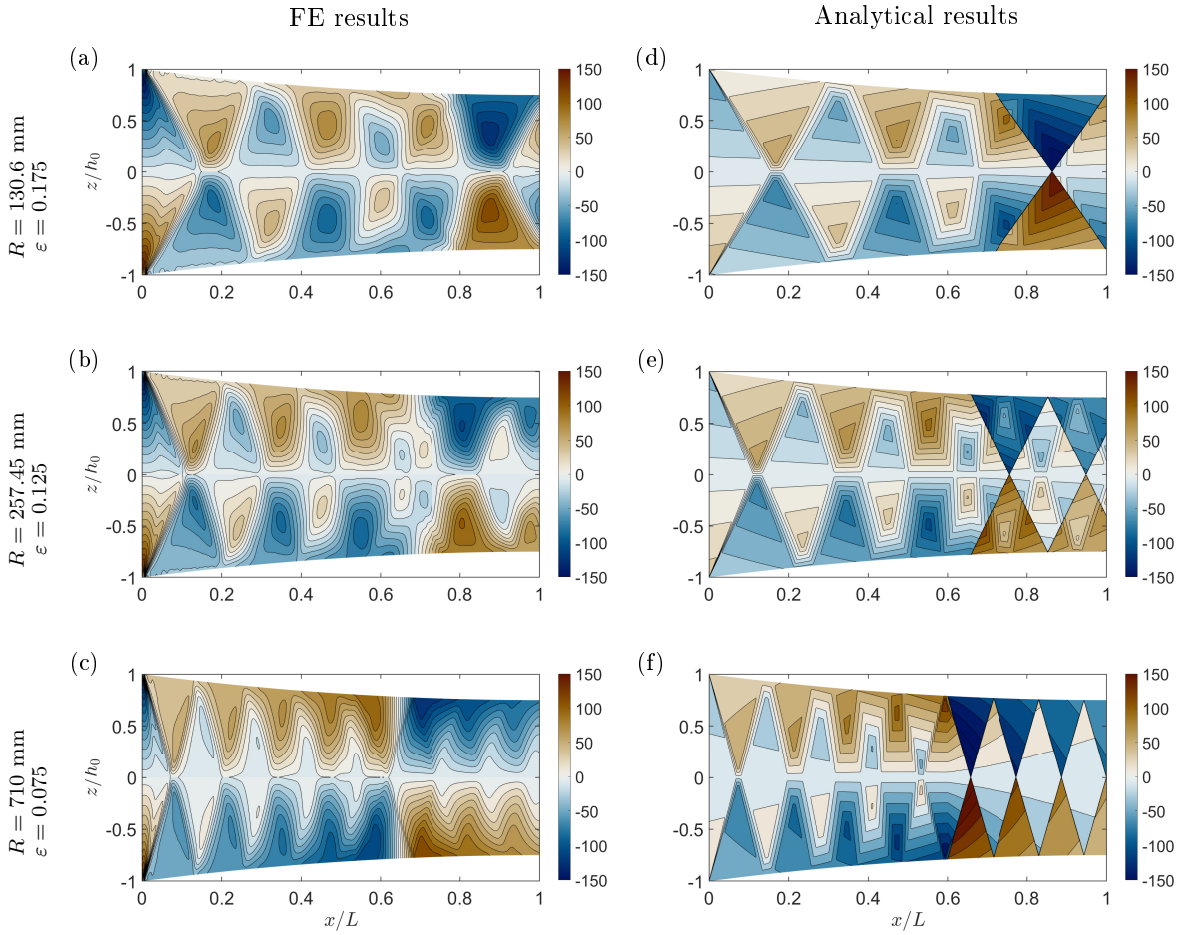

Figure 6: Contour plots of shear stress from simulations with $N_e = 30$ elements. In all cases the stress is measured in MPa. The left panel (a-c) shows FE simulations and the right panel (d-f) shows analytical results from Erfanian et al. (2024) for three different ε values: $\varepsilon = 0.175$ (top row, $R = 130.6\,\text{mm}$), $\varepsilon = 0.125$ (middle row, $R = 257.45\,\text{mm}$) and $\varepsilon = 0.075$ (bottom row, $R = 710\,\text{mm}$). Data is presented inside the roll gap only, between $x/L = 0$ and $x/L = 1$, since Erfanian et al. (2024) do not consider deformations outside the roll gap.

magnitude at the surface and centre of the sheet in Figure 7(c) (solid and dashed curves, respectively). The speed of the roller (black dotted line) is also shown for comparison. According to these curves, the sheet surface initially accelerates when it enters the roll gap and comes into contact with the squeezing roller, as expected from conservation of mass and Coulomb friction. However, the sheet centre does not yet deform under the squeezing effect, and remains at its initial speed. The velocity at the sheet centre does not increase until $x/L \approx 0.1$ while the sheet surface velocity begins to increase at $x/L \approx 0$. From Figure 6 we know that the shear stress has a non-linear distribution through the sheet thickness, and this delayed response to velocity changes is therefore expected. The velocity of the material at the sheet's horizontal centre does not change until the information from the surface reaches the sheet's centre. The acceleration is transmitted to the centre of the sheet via the shear, as shown in Figure 6, so it begins to accelerate later. However, the surface then stops accelerating, in line with the translation-only region (i.e., zero PEEQ rate, as observed in the PEEQ rate results). This means that the mid-surface temporarily accelerates to a faster velocity than the surface. This behaviour is, again, somewhat unexpected, since one might intuitively expect the material velocity to be highest near the sheet surface, where the forcing is imposed. The pattern then repeats, and both regions move through consecutive intervals of acceleration and rigid translation, with the respective velocities leap-frogging each other repeatedly. Furthermore, we observe that one of the velocity plateaus on the surface coincides with the roll velocity, so a "stick" region emerges naturally around the neutral point[2]. This allows the shear stress to smoothly change from positive to negative on the surface as the sheet sticks to the rollers for a small portion of the roll gap, as was observed at the sheet's surface near the neutral point in the FE results in Figure 6.

[2]The neutral point is defined as the position at which the sheet surface speed surpasses the roller speed and hence shear due to friction changes direction (see e.g. $x \approx 0.6$ in Figure 6c).

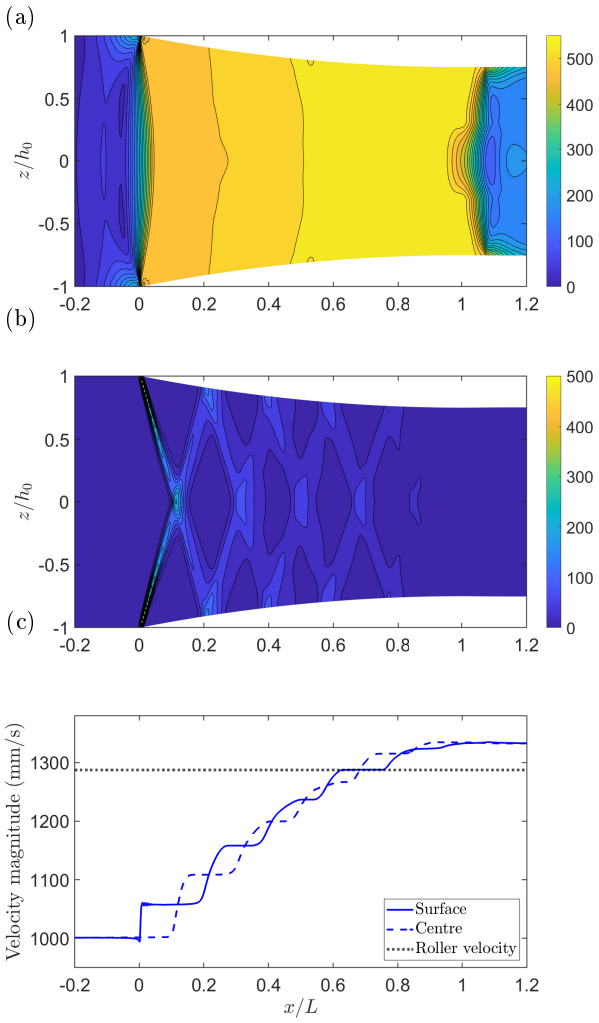

Figure 7: (a) Von Mises stress (MPa), (b) PEEQ rate (s^{-1}) and (c) velocity profiles for the simulation presented in Figure 6(b) ($R = 257.45\,\text{mm}$, $\varepsilon = 0.125$). The PEEQ rate and velocity values are obtained through postprocessing of the PEEQ values and displacements respectively (see Supplementary Material for details of postprocessing).

4.2. Residual stress

The through-thickness variation of the stress inside the roll gap illustrated in Figure 7(a) has a knock-on effect on the residual stress after rolling. In Figure 8(a) we consider a symmetric simulation with a roller radius $R = 32\,\text{mm}$ ($\varepsilon = 0.354$), and all other parameters the same as described in Section 3, and include data from the region $x/L > 1$, i.e. beyond the roll gap. The von Mises stress here gives an indication of the residual stress. We observe distinct zones in the sheet centre and near its surfaces, with maximal von Mises stress in the zones just under the surface. Cross-checking against the individual stress components reveals that the central zone experiences lengthwise compression while the outer zones are under longitudinal tension; this is consistent with longitudinal stress results reported by Tadić et al. (2023).

We also consider asymmetric rolling, and attempt to predict associated curvature. In Figure 8(b), we consider a version of the system in Figure 8(a), but with the speed of the top roller increased by 2.5%.[3]. Large amounts of residual stress are observed in the asymmetric von Mises results, similar to the symmetric case. The magnitude of the residual stress in the sheet for $x/L > 1$ is greater towards the bottom of the sheet, and the sheet's curvature is towards the slower roller for this specific set of parameters. We do not suggest that curvature is always towards the slower roller because, as pointed out by Minton and Brambley (2017), many authors have given contradicting prediction rules for curvature during asymmetric rolling. Rather we hypothesise that the oscillatory pattern in stress and strain quantities presented here, which is largely absent in the literature, influences the through-thickness residual stress profile for $x/L > 1$ and in turn the curvature of the rolled sheet. Indeed, the shifting of the oscillatory pattern as parameters are varied likely explains the inconsistent and poorly-understood trends in curvature reported in the literature (Minton and Brambley, 2017). This is an important aspect of modelling rolling since unintentional asymmetries cause turn-up and turn-down in sheet rolling which can halt the process or even damage the rolling table and mills, and since asymmetries are intentionally exploited in asymmetrical rolling to improve process efficiency and produce curved products (Minton and Brambley, 2017).

5. Physical interpretation and further validation

5.1. Physical interpretation

We interpret the oscillatory pattern presented in Section 4 using insights from the mathematical analysis of Erfanian et al. (2024). To build this interpretation, we need the following key components:

- **Stress and shear axes:** For a long thin roll gap with a small friction coefficient, the principal stresses are tension along the sheet axis and compression through the thickness. The shear axes are then offset by 45° from the principal stresses, i.e. along diagonals in the sheet. For plane strain, in the limit of a rigid-plastic material, these diagonal lines of maximum shear are slip lines. More generally, we expect to see substantial plastic flow along these lines when the material is at yield.

- **Jump in stress:** When the metal sheet moves into contact with the rollers, there is a rapid change in applied stress at the sheet surface: this surface transitions from a stress-free state to experiencing a compressive normal force from the squeezing of the rollers. This jump in stress state is the source of

[3] In this simulation we could not exploit symmetry to achieve the mesh density used in previous simulations, so used 40 elements through-thickness.

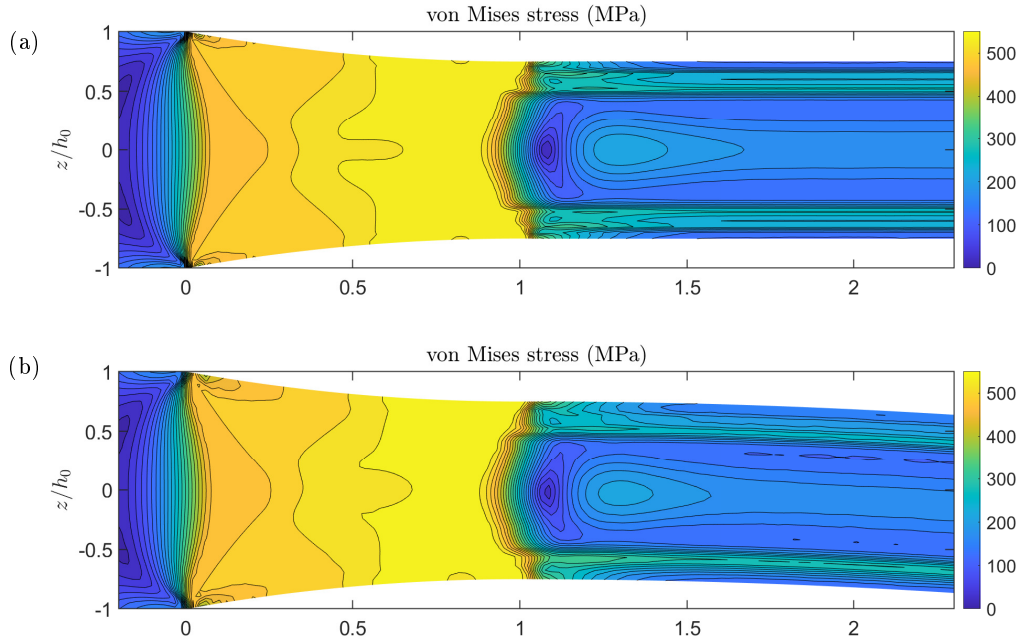

Figure 8: Contour plots of von Mises stress from FE simulations with (a) symmetric and (b) asymmetric roller speeds. The roller radius is $R = 32\,\text{mm}$, corresponding to $\varepsilon = 0.354$. In (a), the tangential velocity of both rollers is $R\Omega = 1287.25\,\text{mm}\,\text{s}^{-1}$, and symmetry is exploited with $N_e = 30$ elements through-half-thickness. In (b), the tantential velocity of the bottom roller is $R\Omega = 1287.25\,\text{mm}\,\text{s}^{-1}$, and the top roller rotates 2.5% faster. Here, the full sheet is modelled with $2N_e = 40$ elements through-thickness.

all of the shear lobes that occur downstream of this point.

We begin by considering the rigid–plastic case illustrated in Figures 6(d–f). The sheet surface undergoes a sudden jump from stress-free to compressed and sheared at the top left and bottom left corners of these plots, with the rollers applying a squeezing force that pushes the outer surfaces of the sheet in towards its mid-surface. This creates a shear wave, which is transmitted along the shear axes of the sheet, i.e. at 45° to the inlet. Tracking at a 45° angle from the top-left corner, we see a slip line along which material will slip downward and to the right. This continues until the slip line hits the bottom surface of the sheet, at which point it is reflected up and to the right, and material is pulled in this new direction. Since the slip lines are oriented at 45° to the horizontal, increasing the length–thickness ratio of the roll gap simply increases the number of reflections that occur inside that space.

Moving our attention now to the elastic–plastic FE cases illustrated in Figures 6(a–c), we observe a modified version of the same pattern. Because the sheet modelled by our FE is elastic-plastic, the shear axes deviate slightly from 45° and the transitions across these axes are smoother. However, plastic flow is still localized around the shear lobe boundaries, as illustrated by the PEEQ rate plot in Figure 7(b). Furthermore, the zig-zag shape of these zones of plastic deformation explain the step-wise velocity illustrated in Figure 7: the velocity of the material increases rapidly when it moves through a zone of high PEEQ rate, and then remains approximately constant until it reaches the next high-PEEQ zone. This occurs depite the fact that the material is at yield throughout the roll gap. We note that an alternative way of visualizing the axes of strain localization is to plot contours of $p \pm 2\theta Y/\sqrt{3}$, where the pressure p is minus the isotropic part of the stress tensor and θ is the anticlockwise rotation angle of the stress element from the positive x-axis for which the stress is in a state of pure shear (Flanagan, 2025, Chapter 2).

Finally, we draw a loose analogy between the pattern observed here and the wake of a ship in a narrow channel. When water flows past the bow of a boat, there is a sudden change in stress at the point where the water is cut by the bow and pushed outward. This generates a wake, which emanates from the bow at approximately 45°. If the boat is in a narrow channel, the wake will then reflect off the channel walls, and bounce over and back across the channel diagonally. In a similar fashion, we can interpret the oscillations in our system as a wake emanating from the point where the metal sheet suddenly meets the rollers.

5.2. Validation against mathematical analysis

The analytical method developed in Erfanian et al. (2024) uses the method of multiple scales and yields a wave-like solution for the stresses in the sheet. This multiple-scales model is valid in the limit where the roll gap is very long and thin, i.e. for $\varepsilon \to 0$. We compare our FE predictions of shear stress with the multiple-scales

prediction by comparing the left and right columns of Figure 6. As Erfanian et al. (2024) do not consider deformations outside the roll gap, our attention here is restricted to values of x/L between 0 and 1 (see Figure 1 for the domain definition). Both methods predict repeating lobes of high and low shear stress, as outlined above. The number and position of lobes predicted by the two methods are in agreement for each value of ε, and the magnitude of shear stress at various through-thickness positions is, in general, comparable. There are some differences between the predictions from the two methods, which we outline and explain now.

5.2.1. *Through-thickness shear profile*

One notable difference between the FE and analytic models is in the shear profiles, which can be seen between the neutral point and the end of the roll gap. In Figure 6 the neutral point is observed in the range $x \approx 0.6L$–$0.75L$ in all contour plots as the x-position at which the shear changes sign on the surface of the sheet. In the FE results, shear stress on the surface varies in a smooth fashion while the analytical model demonstrates a distinct discontinuity in shear stress. The discontinuous change in shear stress seen in the analytical model is due to the slipping Coulomb friction law that is employed. In reality, material sticks to the roller around the neutral point (as shown in Figure 7c above) and shear stress changes sign smoothly (Cawthorn et al., 2016; Domanti and McElwain, 1995). This sticking region around the neutral point is predicted in our FE results, but not in the rigid-plastic analytical model.

5.2.2. *Stick–slip region*

Coulomb friction is employed in our FE model, but frictional constraints are enforced with the stiffness (penalty) method. The penalty method permits some relative surface motion (an "elastic slip") when sticking should occur (i.e., when the shear stress is below the critical magnitude for sliding). While the surfaces are "sticking" the magnitude of sliding is limited to this elastic slip. Elastic slip is controlled computationally by a slip tolerance factor γ. In Figure 9 we investigate the effect that varying γ has on the surface shear stress results, and observe that the gradient in surface shear steepens with decreasing γ, but to a finite limiting value that is far from the infinite slope predicted analytically.

Figure 9 also shows that increasing the Young's modulus by a factor of six has a significant effect on the numerically-predicted shear stress on the sheet's surface: the gradient near the neutral point steepens and the position of the neutral point is closer to the position predicted analytically. This is expected as these material parameters more closely resemble rigid-plastic behaviour. This suggests that the friction rule alone is not responsible for the discrepancies between the FE and analytical results in Figure 6, and that the rigid-plastic (i.e., no elastic effects) assumption in the analytical model is also an important contributing factor.

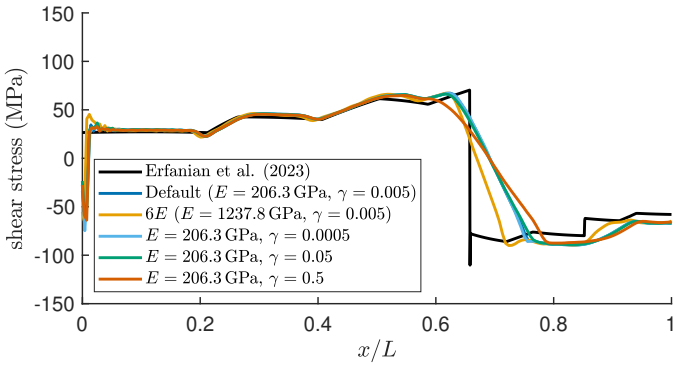

Figure 9: Shear stress along the top surface of the deformed sheet from the analytical model by Erfanian et al. (2024) and from simulations with different Young's modulus (E) and elastic slip tolerance (γ) values. The default values are $E = 206.3\,\text{GPa}$ and $\gamma = 0.005$. All simulations have radius $R = 257.45\,\text{mm}$ and $\varepsilon = 0.125$.

5.3. *Experimental validation*

Transferring the insight from this paper to practical application would be greatly aided by experimental validation. The most suitable experimental results we observed in the literature were the deformation zones illustrated in Fig. 2(a) from Tarnovskii et al. (1965) and the shear strain and vertical velocity measurements in Figure 7(j,e) of Hoefnagels et al. (2022). Both appear to be surface measurements, so limited agreement with our 2D plane-strain model should be expected; nonetheless they are a useful starting point.

The Tarnovskii et al. (1965) measurements are for a sheet whose thickness is close to the roll gap length, so we expect one shear oscillation, corresponding to the distinctive X shape illustrated. Repetition of this (or similar investigations of the interior with rolled plasticine (Orowan, 1943)) for thinner sheets or a longer roll gap would give an excellent resource for validation and for further investigation of the phenomenon uncovered numerically.

The strain and velocity results in Hoefnagels et al. (2022) are obtained using DIC and exhibit only a slight oscillation along the sheet length. If accurate measurements of strain rate could be obtained these would again be a useful resource for validation. However, the DIC process involves fitting observations to polynomials, and the order of the polynomials determines the feature size that can be resolved. Hoefnagels *et al.* use polynomials of order 3 in the thickness direction and order 8 along the length, which is quite likely too low to resolve the patterns of interest to us. It is also worth noting that the standard polynomials used here are particularly poorly suited to fitting oscillatory/periodic behaviour; an alternative such as Chebyshev polynomials might well represent features more clearly with the same number of degrees of freedom.

5.4. Further parameter variation

It is reasonable to ask to what extent the novel patterns presented here are unique to our specific modelling choices. Based on the physical interpretation outlined in §5.1 and the validation against mathematical analysis in §5.2, there is strong evidence that these oscillatory patterns are physically meaningful and not a quirk of the modelling or material properties. Nonetheless, we provide a brief discussion here of how the patterns may change if material properties are modified.

- **Hardening:** In this paper we considered an elastic-plastic model with strain hardening, where the yield stress increases from 477.2 MPa initially to 650.25 MPa at a true plastic strain of 1.1. The presence of this hardening does not change the oscillatory pattern observed in the shear, it only causes a gradual increase in the magnitude of the stresses along the length of the roll gap (Erfanian et al., 2024). This makes sense because the yield stress increases along the roll gap as strain induced by the roller accumulates. We therefore anticipate that increasing the magnitude of the strain hardening would lead to further increases in the magnitude of the stresses but would not significantly change the oscillatory pattern. Other types of hardening, for example with strain-rate dependence, are beyond the scope of the current work.

- **Friction:** For the modelling in this paper we considered Coulomb friction, with a friction coefficient $\mu = 0.1$ selected from a typical range 0.02–0.15. The shear force applied by the rollers to the sheet scales with μ, so if this friction coefficient was reduced the jump in shear stress where the sheet meets the rollers would decrease. However, the jump in compressive normal stress from the squeezing effect of the rollers would remain, and so we would expect the shear lobes to persist, albeit with the possibility of a slight change in their shape or magnitude. The possible exception is near the neutral point, where imposing a Coulomb friction rule exactly leads to an additional jump in shear stress, which affects the shear lobes slightly. For example, increasing the slip tolerance factor leads to a decrease in the sharpness of this jump but does not change the oscillatory pattern elsewhere (cf. Figure 9).

6. Conclusion

FE rolling models in the existing literature are typically limited in their resolution of through-thickness variations. This is important because through-thickness variation of stress and strain can have consequences for microstructure evolution and residual stress. FE specifications such as element types, solver type (implicit versus explicit), and mesh density were investigated here to arrive at the final FE model. This final FE model is a static, implicit model with $N_e = 30$ CPE4R elements employed through the half-thickness of the sheet, significantly more than the $N_e = 5$–10 typically used in common practice today. We show that our through-thickness predictions compare well with a rigid-perfectly-plastic analytical model (Erfanian et al., 2024). Excellent agreement in shear stress was found when comparing the analytical and FE models. Both models captured the oscillatory nature of shear during rolling. The relatively small discrepancies between the shear results of the two models can be attributed to the size of the roll-gap aspect ratio, $1/\varepsilon$ and the differences in the material and friction models, with the analytic model not allowing for a sticking region near the neutral point. In the limits as $\varepsilon \to 0$, $\gamma \to 0$ and $E \to \infty$, we hypothesise that the agreement between the FE and analytical results would be even further improved.

Previous studies have often relied on the convergence of roll force and roll torque to assess the quality of numerical rolling simulations. Here, we show that roll force and roll torque are poor indicators of simulation quality. This is because those averaged quantities often converge well even for under-resolved simulations that fail to accurately predict other quantities of interest such as the through-thickness stress distribution.

Unexpectedly, our results show the existence of a region near the neutral point where the sheet and rollers stick, rather than slip. While care has been taken here to ensure that the sticking region near the neutral point is not a numerical artefact, it is a consequence of how friction is modelled, and this may be an overly-simplified model of the friction that practically occurs in metal rolling. Comparison with the analytical model shows that the effects of this sticking region on the stress oscillation pattern through-thickness are important beyond the neutral point and affects the shear stresses at the roll-gap exit.

All of the analysis here, and many of the previous studies in Table 1, assume plane strain to reduce the problem to 2D. This is valid sufficiently far from the edge of the sheet provided the sheet is sufficiently wide and the rolls are perfectly aligned. However, in order to study edge effects, misalignment of the rolls, or less-wide sheets, a fully 3D study would be needed. A consequence of the analysis here is that $2N_e = 60$ elements through-thickness were needed to accurately resolve through-thickness behaviour, and this level of detail would be extremely computationally expensive in a 3D simulation, especially since, to avoid elements with a large aspect ratio, a comparably large number of across-width elements would presumably also be needed. It may be possible to model very narrow strips and instead assume a plane stress condition to reduce the problem to a (different) 2D model, although this has not been investigated here.

While in this study the FE software ABAQUS was used, we believe the principles described here are applicable to all FE studies, and this could be verified and best practice refined by performing similar studies using other commonly-used softwares. Future work could include employing second-order elements to discretise the metal sheet. Expanding upon the preliminary study in §4.2 of curvature induced by asymmetric rolling might allow for the prediction and control of curvature; the lack of through-thickness resolution may be what has been preventing previous FE studies from correctly predicting curvature from asymmetric rolling (Minton and Brambley, 2017). Further study in this area would likely be enhanced by the use of $p \pm 2\theta Y/\sqrt{3}$ contours provisionally presented in Flanagan (2025).

Acknowledgements

This publication has emanated from research funded by Research Ireland under grant numbers 18/CRT/6049 (Flanagan), 21/FFP-P/10160 (O'Kiely), 13/RC/2094 (O'Connor) and SOWP2-TP0023 (O'Connor), as well as UKRI (MR/V02261X/1, Brambley), the EU (101028291, O'Connor) and a University of Warwick Chancellor's Scholarship (Erfanian). For the purpose of open access, the authors have applied a CC BY public copyright licence to any Author Accepted Manuscript version arising from this submission.

References

E. Orowan, The calculation of roll pressure in hot and cold flat rolling, Proceedings of the Institution of Mechanical Engineers 150 (1943) 140–167.

P. M. Horton, J. M. Allwood, Yield improvement opportunities for manufacturing automotive sheet metal components, Journal of Materials Processing Technology 249 (2017) 78–88.

M. Wehr, D. Stenger, S. Schätzler, R. Beyer, D. Abel, G. Hirt, Online model adaptation in cold rolling for improvement of thickness precision, IFAC-PapersOnLine 53 (2020) 10372–10379.

R. L. Milford, J. M. Allwood, J. M. Cullen, Assessing the potential of yield improvements, through process scrap reduction, for energy and CO_2 abatement in the steel and aluminium sectors, Resources, Conservation and Recycling 55 (2011) 1185–1195.

J. M. Allwood, S. Duncan, J. Cao, P. Groche, G. Hirt, B. Kinsey, T. Kuboki, M. Liewald, A. Sterzing, A. E. Tekkaya, Closed-loop control of product properties in metal forming, CIRP Annals 65 (2016) 573–596.

World Steel Association, World Steel in Figures 2024, Technical Report, World Steel Association, 2024. URL: https://worldsteel.org/wp-content/uploads/World-Steel-in-Figures-2024.pdf.

I. Tarnovskii, A. Pozdeyev, V. Lyashkov, Deformation of metals during rolling (English edition), Pergamon Press, 1965.

M. Erfanian, E. J. Brambley, F. Flanagan, D. O'Kiely, A. N. O'Connor, Through-thickness modelling of metal rolling using multiple-scale asymptotics, 2024. URL: https://arxiv.org/abs/2408.01347. arXiv:2408.01347.

P. Montmitonnet, L. Fourment, U. Ripert, Q. Ngo, A. Ehrlacher, State of the art in rolling process modelling, BHM Berg-und Hüttenmännische Monatshefte 161 (2016) 396–404.

Z. Hu, Z. Wei, H. Sun, J. Yang, L. Wei, Optimization of metal rolling control using soft computing approaches: a review, Archives of Computational Methods in Engineering 28 (2021) 405–421.

J. Minton, C. Cawthorn, E. Brambley, Asymptotic analysis of asymmetric thin sheet rolling, International Journal of Mechanical Sciences 113 (2016) 36–48.

E. G. Thompson, Inclusion of elastic strain rate in the analysis of viscoplastic flow during rolling, International Journal of Mechanical Sciences 24 (1982) 655–659.

K. Mori, K. Osakada, T. Oda, Simulation of plane-strain rolling by the rigid-plastic finite element method, International Journal of Mechanical Sciences 24 (1982) 519–527.

I. Yarita, R. L. Mallett, E. H. Lee, Stress and deformation analysis of plane-strain rolling process, Steel Research 56 (1985) 255–259.

A. Lau, R. Shivpuri, P. Chou, An explicit time integration elastic-plastic finite element algorithm for analysis of high speed rolling, International journal of mechanical sciences 31 (1989) 483–497.

M. Yoshii, K. Ohmori, T. Seto, H. Nikaido, H. Nishizaki, M. Inoue, Analysis of warping phenomenon in plate rolling, ISIJ International 31 (1991) 973–978.

A. B. Richelsen, Elastic—plastic analysis of the stress and strain distributions in asymmetric rolling, International Journal of Mechanical Sciences 39 (1997) 1199–1211.

S. Ghosh, M. Li, D. Gardiner, A computational and experimental study of cold rolling of aluminum alloys with edge cracking, J. Manuf. Sci. Eng. 126 (2004) 74–82.

P. Gudur, U. Dixit, A neural network-assisted finite element analysis of cold flat rolling, Engineering Applications of Artificial Intelligence 21 (2008) 43–52.

J. G. Lenard, Primer on flat rolling, Newnes, 2013.

C. J. Cawthorn, E. G. Loukaides, J. M. Allwood, Comparison of analytical models for sheet rolling, Procedia Engineering 81 (2014) 2451–2456.

J. Minton, Mathematical modelling of asymmetrical metal rolling processes, Ph.D. thesis, University of Cambridge, 2017.

P. Hartley, C. Sturgess, C. Liu, G. Rowe, Experimental and theoretical studies of workpiece deformation, stress, and strain during flat rolling, International materials reviews 34 (1989) 19–34.

C. Boldetti, C. Pinna, I. Howard, G. Gutierrez, Measurement of deformation gradients in hot rolling of aa3004, Exp. Mech. 45 (2005) 517–525.

L. Jacobs, K. Van Dam, D. Wentink, M. De Rooij, J. Van Der Lugt, D. Schipper, J. Hoefnagels, Effect of asymmetric material entrance on lubrication in cold rolling, Tribol. Int. 175 (2022) 107810.

J. Hoefnagels, K. Van Dam, N. Vonk, L. Jacobs, Accurate strain field measurement during strip rolling by exploiting recurring material motion with time-integrated digital image correlation, Exp. Mech. 62 (2022) 603–625.

L.-E. Lindgren, J. Edberg, Explicit versus implicit finite element formulation in simulation of rolling, Journal of Materials Processing Technology 24 (1990) 85–94.

A. B. Richelsen, Comparison of a numerical analysis of rolling with experimental data, Journal of materials processing technology 57 (1996) 70–78.

C. Cawthorn, J. Minton, E. Brambley, Asymptotic analysis of cold sandwich rolling, International Journal of Mechanical Sciences 106 (2016) 184–193.

M. Erfanian, E. J. Brambley, F. Flanagan, D. O'Kiely, A. O'Connor, New models for cold rolling: Generalized slab theory and slip lines for fast predictions without finite elements, in: International Conference on the Technology of Plasticity, Springer, 2023, pp. 223–233.

F. Flanagan, D. O'Kiely, A. O'Connor, M. Erfanian, E. J. Brambley, New discoveries in cold rolling: Understanding stress distribution and parameter dependence for faster, more accurate models, in: International Conference on the Technology of Plasticity, Springer, 2023, pp. 211–222.

O. Olaogun, J. Edberg, L.-E. Lindgren, O. Oluwole, E. Akinlabi, Heat transfer in cold rolling process of AA8015 alloy: a case study of 2-D FE simulation of coupled thermo-mechanical modeling, The International Journal of Advanced Manufacturing Technology 100 (2019) 2617–2627.

P. Howell, G. Kozyreff, J. Ockendon, Applied solid mechanics,

Cambridge University Press, 2009.
C. Liu, P. Hartley, C. Sturgess, G. Rowe, Finite-element modelling of deformation and spread in slab rolling, International journal of mechanical sciences 29 (1987) 271–283.
N. Tadić, M. Mišović, Ž. Radović, An analysis of longitudinal residual stresses in en aw-5083 alloy strips as a function of cold-rolling process parameters, Journal of the Mechanical Behavior of Materials 32 (2023) 20220297.
G.-J. Li, S. Kobayashi, Rigid-plastic finite-element analysis of plane strain rolling, Journal of Manufacturing Science and Engineering (1982).
C. Liu, P. Hartley, C. Sturgess, G. Rowe, Analysis of stress and strain distributions in slab rolling using an elastic-plastic finite-element method, International journal for numerical methods in engineering 25 (1988) 55–66.
M. Misovic, N. Tadic, M. Jacimovic, M. Janjic, Deformations and velocities during the cold rolling of aluminium alloys, Materiali in tehnologije 50 (2016) 59–67.
J. D. Murray, Asymptotic analysis, volume 48, Springer Science & Business Media, 2012.
C. Liu, P. Hartley, C. Sturgess, G. Rowe, Elastic-plastic finite-element modelling of cold rolling of strip, International journal of mechanical sciences 27 (1985) 531–541.
K. Mori, K. Osakada, Analysis of the forming process of sintered powder metals by a rigid-plastic finite-element method, International journal of mechanical sciences 29 (1987) 229–238.
Z. Malinowski, J. Lenard, A study of the state of stress during cold striprolling, Journal of Materials Processing Technology 33 (1992) 273–288.
A. Shahani, S. Setayeshi, S. Nodamaie, M. Asadi, S. Rezaie, Prediction of influence parameters on the hot rolling process using finite element method and neural network, Journal of materials processing technology 209 (2009) 1920–1935.
L. Zhou, Z. Huang, C. Wang, X. Zhang, B. Xiao, Z. Ma, Constitutive flow behaviour and finite element simulation of hot rolling of SiCp/2009Al composite, Mechanics of Materials 93 (2016) 32–42.
B. Koohbor, K. Moaven, Finite-element modeling of thermal aspects in high speed cold strip rolling, Proceedings of the Institution of Mechanical Engineers, Part B: Journal of Engineering Manufacture 231 (2017) 1350–1362.
S. Domanti, D. McElwain, Two-dimensional plane strain rolling: an asymptotic approach to the estimation of inhomogeneous effects, International journal of mechanical sciences 37 (1995) 175–196.
A. Hadadian, R. Sedaghati, Investigation on thermal relaxation of residual stresses induced in deep cold rolling of Ti–6Al–4V alloy, The International Journal of Advanced Manufacturing Technology 100 (2019) 877–893.
Dassault Systémes, SIMULIA User Assistance 2021 Abaqus, 2021.
Z. Jiang, A. Tieu, Elastic–plastic finite element method simulation of thin strip with tension in cold rolling, Journal of Materials Processing Technology 130 (2002) 511–515.
P. Natário, N. Silvestre, D. Camotim, Web crippling failure using quasi-static FE models, Thin-Walled Structures 84 (2014) 34–49.
E. Gavalas, I. Pressas, S. Papaefthymiou, Mesh sensitivity analysis on implicit and explicit method for rolling simulation, International Journal of Structural Integrity 9 (2018) 465–474.
N. Padhye, Mechanics and modeling of cold rolling of polymeric films at large strains—a rate-independent approach, Mechanics of Materials 184 (2023) 104733.
W. Min, Y. He, Z.-C. Sun, L.-g. Guo, X.-z. Ou, Dynamic explicit FE modeling of hot ring rolling process, Transactions of Nonferrous Metals Society of China 16 (2006) 1274–1280.
A. Ktari, Z. Antar, N. Haddar, K. Elleuch, Modeling and computation of the three-roller bending process of steel sheets, Journal of mechanical science and technology 26 (2012) 123–128.
J. Edberg, L.-E. Lindgren, Efficient three-dimensional model of rolling using an explicit finite-element formulation, Communications in numerical methods in engineering 9 (1993) 613–627.
A. Díaz, I. Cuesta, J. Alegre, A. de Jesus, J. Manso, Residual stresses in cold-formed steel members: Review of measurement methods and numerical modelling, Thin-Walled Structures 159 (2021) 107335.
D. Jung, D.-Y. Yang, Step-wise combined implicit–explicit finite-element simulation of autobody stamping processes, Journal of Materials Processing Technology 83 (1998) 245–260.
A. Hacquin, P. Montmitonnet, J.-P. Guillerault, A steady state thermo-elastoviscoplastic finite element model of rolling with coupled thermo-elastic roll deformation, Journal of materials processing technology 60 (1996) 109–116.
C. Yao, A. He, J. Shao, J. Zhao, A real-time quasi-3d metal flow model for hot strip rolling, International Journal of Mechanical Sciences 159 (2019) 91–102.
C. Yao, A. He, J. Shao, J. Zhao, G. Zhou, H. Li, Y. Qiang, Finite difference modeling of the interstand evolutions of profile and residual stress during hot strip rolling, Metals 10 (2020) 1417.
L. Jacobs, E. Atzema, J. Moerman, M. de Rooij, Quantification of the influence of anisotropic plastic yielding on cold rolling force, Journal of Materials Processing Technology 319 (2023) 118055.
M. Spittel, T. Spittel, Steel symbol/number: Dc04/1.0338: Metal forming data-ferrous alloys-deformation behaviour, Metal Forming Data of Ferrous Alloys-deformation behaviour (2009) 162–167.
X. Shangwu, J. Rodrigues, P. Martins, Simulation of plane strain rolling through a combined finite element–boundary element approach, Journal of Materials Processing Technology 96 (1999) 173–181.
M. Safaei, W. De Waele, Towards better finite element modelling of elastic recovery in sheet metal forming of advanced high strength steel, in: Sustainable Construction and Design 2011 (SCAD), volume 2, Ghent University, Laboratory Soete, 2011, pp. 217–227.
H. Qiao, M. Barnett, P. Wu, Modeling of twin formation, propagation and growth in a Mg single crystal based on crystal plasticity finite element method, International Journal of Plasticity 86 (2016) 70–92.
E. Q. Sun, Shear locking and hourglassing in MSC Nastran, ABAQUS, and ANSYS, in: Msc software users meeting, 2006, pp. 1–9.
C. D. Souto, A. Menghini, A. Diaz, J. M. Manso, A. M. de Jesus, C. A. Castiglioni, Determination of manufacturing residual stresses in cold-formed thin-walled steel profiles, Thin-Walled Structures 180 (2022) 109945.
H. Zhang, G. Liu, N. Guo, X. Meng, Y. Shi, H. Su, Z. Liu, B. Tang, Damage evolution of hot stamped boron steels subjected to various stress states: Macro/micro-scale experiments and simulations, Materials 15 (2022) 1751.
Z. Yang, X. Deng, Z. Li, Numerical modeling of dynamic frictional rolling contact with an explicit finite element method, Tribology international 129 (2019) 214–231.
S. Matsubara, A. Ogino, S. Nagashima, D. Okumura, Computational and physical aspects for the occurrence of crease in an elastomer under general loading conditions, International Journal of Solids and Structures 288 (2024) 112610.
S. Gao, J. Yang, Y. Xu, Y. Zhang, Q. Bai, Effect of dynamic constitutive differences in materials on the impact performance of cfst via secondary development of abaqus, in: Structures, volume 62, Elsevier, 2024, p. 106236.
X. Qian, W. Chengguo, G. Ge, The research of parallel computing for large-scale finite element model of wheel/rail rolling contact, in: 2010 3rd International Conference on Computer Science and Information Technology, volume 1, IEEE, 2010, pp. 254–257.
T. Mang, Encyclopedia of lubricants and lubrication, volume 1, Springer Berlin Heidelberg, 2014.
J. Minton, E. Brambley, Meta-analysis of curvature trends in asymmetric rolling, Procedia engineering 207 (2017) 1355–1360.
F. Flanagan, Mathematical modelling of the cold-rolling process, Ph.D. thesis, University of Limerick, 2025.